Vanadium Dioxide Cathodes for High-Rate Photo-Rechargeable Zinc-Ion Batteries

Buddha Deka Boruah,* Angus Mathieson, Sul Ki Park, Xiao Zhang, Bo Wen, Lifu Tan, Adam Boies, and Michael De Volder*

Photovoltaics are an important source of renewable energy, but due to the intermittent nature of insolation, solar cells usually need to be connected to rechargeable batteries, electrochemical capacitors or other energy storage devices, which adds to the complexity and cost of these systems. In this work, a cathode design for photo-rechargeable zinc-ion batteries (photo-ZIBs) is reported, that is inherently capable of harvesting sunlight to recharge without the need for external solar cells. The proposed photocathodes, comprising a composite of vanadium dioxide nanorods and reduced graphene oxide, are engineered to provide the necessary charge separation and storage for photocharging under illumination. The photo-ZIBs achieve capacities of ≈ 282 mAh g^{-1} in the dark and ≈ 315 mAh g^{-1} under illumination, at 200 mA g^{-1}, demonstrating the use of light not only to charge the devices, but additionally to enhance their capacity. The photo-ZIBs also demonstrate enhanced high-rate capabilities under illumination, as well as a capacity retention of $\approx 90\%$ over 1000 cycles. The proposed photo-ZIBs are considered a promising new technology for addressing energy poverty, due to their high performance and inherent cost-efficiency and safety.

1. Introduction

The development of off-grid energy harvesting and storage systems is important to power stand-alone sensors and other autonomous devices as well as for addressing energy poverty in developing countries. Solar cells are oftentimes used in conjunction with batteries or supercapacitors to smooth out the intermittent nature of insolation, and interesting research has recently been undertaken in the integration of energy harvesting and storage technologies.[1–4] However, combining solar cells with

Dr. B. Deka Boruah, A. Mathieson, Dr. S. K. Park, Dr. X. Zhang, B. Wen, L. Tan, Dr. A. Boies, Prof. M. De Volder
Department of Engineering
University of Cambridge
Cambridge CB3 0FS, UK
E-mail: bd411@cam.ac.uk; mfld2@cam.ac.uk
A. Mathieson, B. Wen, L. Tan
Cambridge Graphene Centre
University of Cambridge
Cambridge CB3 0FA, UK

The ORCID identification number(s) for the author(s) of this article can be found under https://doi.org/10.1002/aenm.202100115.

electrochemical energy storage devices typically requires electronics to match the output of the energy harvester to the requirements of the storage systems.[5,6] This approach also adds to the device complexity and ohmic contact losses.[5,6] To try and avoid these issues, researchers have developed redox flow,[7,8] lithium-air batteries,[9,10] aqueous rechargeable batteries,[11] and electrochemical capacitors[12,13] that can be recharged directly when exposed to light. More recently, lithium-ion batteries (LIBs)[6,14,15] that can be recharged by light only, eliminating the need of any external solar cells have been demonstrated. While impressive, these systems often suffer from low capacities, poor cycling stability, and low energy conversion efficiency. In addition, these have only been tested in half-cells against Li metal.

Our research group recently reported a photo-rechargeable zinc-ion battery (photo-ZIB)[5] device that goes some way in addressing the above challenges and achieved conversion efficiencies of 1.2%, capacities of ≈ 140 mAh g^{-1}, a capacity retention of $\approx 83\%$ over 500 cycles, and relied on P3HT to support that photo-generated charge separation process. In addition, the use of Zn metal anodes provide greater device stability and safety compared to those using Li metal anodes. Here, we report a photo-ZIB cathode using a simple mixture vanadium dioxide (VO$_2$) and reduced graphene oxide (rGO). These electrodes have a capacity of 282 mAh g^{-1} (at 200 mA g^{-1}), which is about two times higher than that of our previously reported photo-ZIB and they achieve a higher rate capability. In addition, the VO$_2$ cathodes reported here have a better capacity retention of $\approx 90\%$ over 1000 cycles. Finally, in this work rGO is used in place of P3HT, which might reduce the overall cost of the device.

Figure 1a illustrates the proposed photocharging mechanism of the photo-ZIB, using VO$_2$ cathodes mixed with rGO. The photocathodes are designed to enable efficient separation and transportation of the photo-generated charges necessary to yield the photocharging effect (see further). The VO$_2$ nanorods are synthesized using a hydrothermal microwave synthesis as described in the Experimental Section. Figure 1b shows a scanning electron microscope (SEM) image of the VO$_2$ nanorods, which have an interplanar spacing of ≈ 0.35 nm (see Figure 1c that corresponds to (110) planes of VO$_2$(B) monoclinic structure).[16,17] Figure 1d shows the energy dispersive X-ray spectroscopy (EDS) spectrum of a nanorod, with the

ADVANCED
SCIENCE NEWS
www.advancedsciencenews.com

ADVANCED
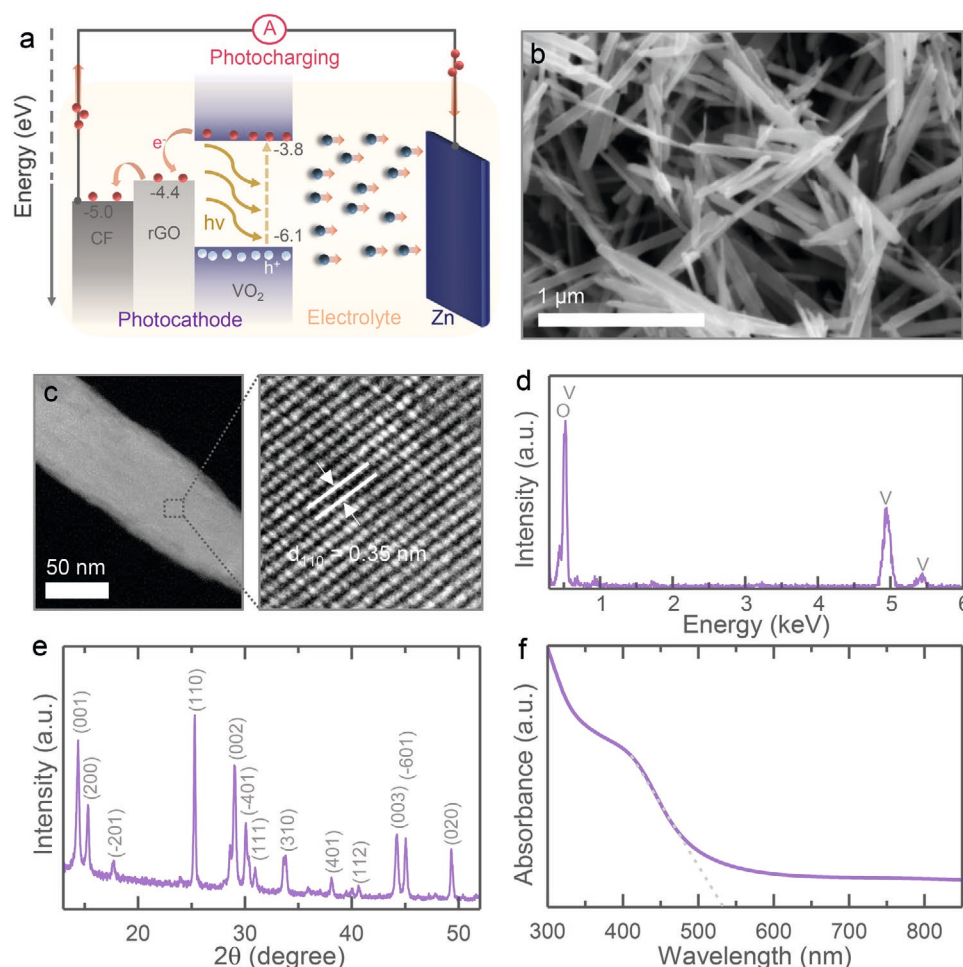**ENERGY**
MATERIALS
www.advenergymat.de

Figure 1. a) Schematic illustration of the proposed photocharging mechanism of VO_2–rGO photo-ZIBs. b) SEM image of the as-synthesized VO_2 nanorods used in the photocathodes. c) Transmission electron microscopy and high-resolution transmission electron microscopy images of a VO_2 nanorod showing the expected lattice spacing. d) EDS spectrum of a VO_2 nanorod. e,f) Powder XRD pattern and UV–VIS absorption spectrum of the VO_2 nanorods.

relevant elemental mappings shown in Figure S1, Supporting Information. The X-ray powder diffraction (XRD) pattern of the VO_2 nanorods is provided in Figure 1e and can be indexed to the monoclinic VO_2 (B) phase with space group of C2/m,[16,17] and finally, UV–VIS absorption spectroscopy shows an indirect bandgap and direct bandgap energies of ≈2.3 and ≈2.53 eV (Figure 1f, Figure S2, Supporting Information).

To support the separation of photo-excited charges in the photo-ZIB cathode, the addition of rGO in the electrode is critical to obtain a favorable energy pathway, as depicted in Figure 1a. To confirm this mechanism, the optical sensitivity and charge separation/transportation between VO_2 and rGO are studied by investigating the light response of various photodetector (PD) based device structures (details of the PD fabrication and electrical measurements are provided in the Experimental Section). **Figure 2**a shows current–voltage (IV) curves in dark and light conditions for a PD using gold (Au) interdigitated electrodes (IDE) on which VO_2 nanorods are cast (digital photograph of the PD provided in Figure S3a, Supporting Information). The increase in output current under illumination (photocurrent) as compared to dark, confirms the

photosensitivity of our VO_2 nanorods in this device architecture. The currents in dark and light intersect at 0 V, suggesting the need for an external bias to separate photogenerated electrons and holes in VO_2. The current–time PD measurements in light and dark conditions with a bias voltage of 1 V are shown in Figure 2b to demonstrate this. In addition, we tested PDs consisting of layer-by-layer rGO/VO_2 structures deposited on fluorine doped tin oxide (FTO) substrates to yield a PD FTO/rGO/VO_2/silver (Ag) stack (see Figure S3b, Supporting Information). Importantly, these PDs show photocurrent even in absence of external bias voltage ($V = 0$ V) under illumination (Figure 2c). This indicates that this material stack is capable of both generating and separating photo-generated charges, without the need for an external bias, much like a solar-cell device. The generated in-built electric field in between VO_2 and rGO is therefore deemed sufficient to separate the photogenerated electrons and holes by transporting electrons from VO_2 to the rGO. The photocurrent measurements at $V = 0$ V (Figure 2d) can be explained from the energy band diagram in Figure 2e which illustrates the electron–hole pair generation, separation, and transportation—electrons from VO_2 to rGO and then to FTO and holes
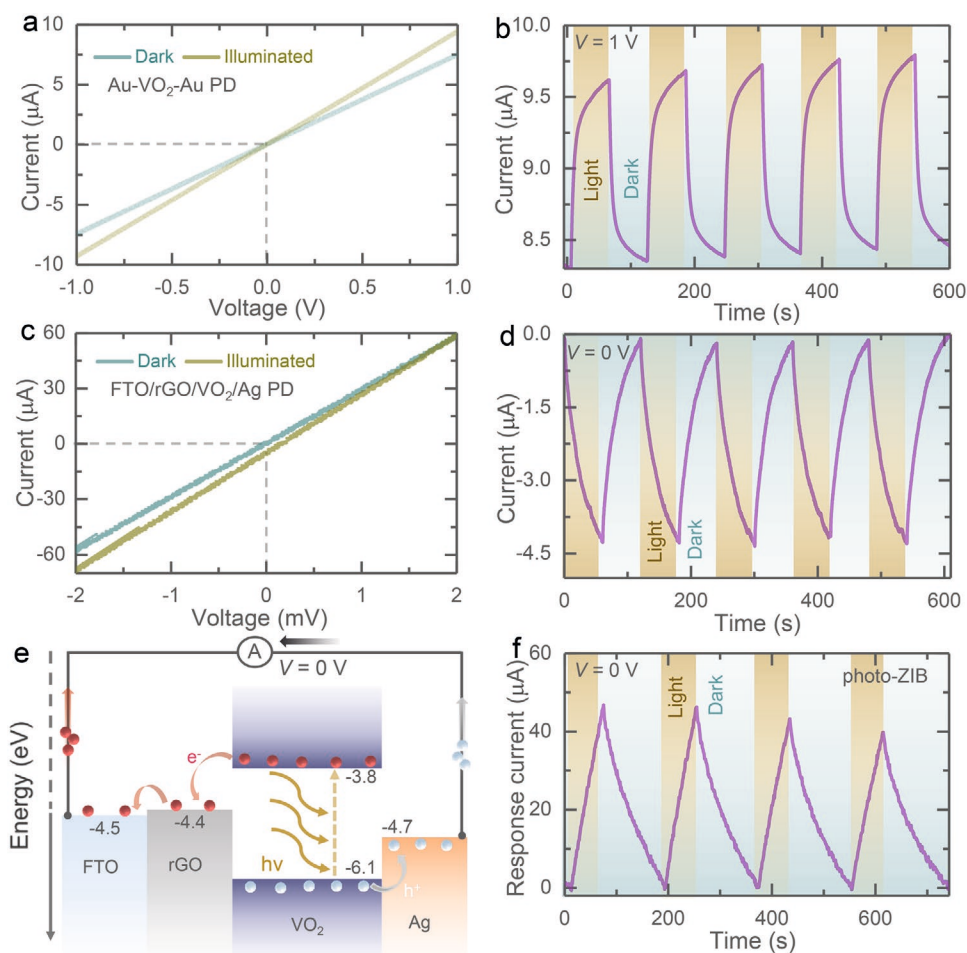
ADVANCED
SCIENCE NEWS
www.advancedsciencenews.com

ADVANCED
ENERGY
MATERIALS
www.advenergymat.de

Figure 2. a) IV curves of a PD using Au—VO$_2$—Au IDE in dark and illuminated conditions ($\lambda \approx$455 nm). b) Current–time measurements of the PD under alternating dark and illuminated conditions at 1 V applied bias voltage. c) IV curves of a stacked FTO/rGO/VO$_2$/Ag PD in dark and illuminated conditions ($\lambda \approx$455 nm). d) Current–time measurements of the stacked PD under alternating dark and light conditions (at 0 V bias voltage). e) Energy band diagram of the stacked PD design. f) Chronoamperometry measurement of the photo-ZIB under alternating dark and illuminated conditions ($\lambda \approx$455 nm, intensity $\approx$12 mW cm^{-2}, 0 V applied voltage).

from VO$_2$ to the Ag electrode. The experimental estimation of energy bands positions of our VO$_2$ nanorods is included in Supporting Information (Figure S4 and Table S1, Supporting Information). In photo-ZIB devices, layer-by-layer deposition of the rGO and VO$_2$ is not practical and therefore the two materials are simply mixed and dropcasted together on a carbon felt (CF) current collector, with the addition of a polyvinylidene fluoride (PVDF) binder (see Experimental Section). However, the aggregate motion of the photocharges still follows the same process as demonstrated in the PD device. Chronoamperometry measurements on these mixed battery electrode formulations in dark and illuminated conditions, show an increase in the response current under light (=$I_{ph}-I_d$; where I_d and I_{ph} are the currents in dark and light, respectively). This supports the hypothesis that the mixed photocathodes still support the proposed charge separation and photocharging mechanism (Figure 2f).

Coin cells (CR2450) with a $\approx$8 mm diameter glass window for light access are constructed (see Experimental Section) for light charging tests. The VO$_2$ based photocathodes are tested against Zn metal anodes (this corresponds to a full cell configuration

for Zn-ion batteries) using a glass microfiber separator soaked in aqueous 3 M Zn(CF$_3$SO$_3$)$_2$ electrolyte (see Experimental Section). First, we measure cyclic voltammograms (CV) at different scan rates (0.2–10 mV s^{-1}) within a voltage window of 0.2–1.4 V and compare the results from dark and illuminated conditions. An LED light source with a central wavelength of $\approx$455 nm and intensity of $\approx$12 mW cm^{-2} is used for all light-exposure experiments, unless specified otherwise. The baseline CV responses of the photo-ZIB, for the different scan rates in the dark conditions are shown in **Figure 3**a. Two cathodic peaks (labeled Peak 1 and Peak 2) along with the corresponding anodic peaks (Peak 3 and Peak 4) are observed, corresponding to different intercalation and deintercalation reactions, which have been reported previously.[17,18] The magnitude of the peak current, for all peaks, clearly increases under illumination (Figure 3b) in addition to there being a slight reduction in the over potential. The CV response, by area, increases by 37.4% at 1 mV s^{-1} when under illumination compared to dark (Figure 3c), and enhances by $\approx$110% at 10 mV s^{-1} (Figure 3d); Figures S5 and S6, Supporting Information, show the CV curves at higher scan rates
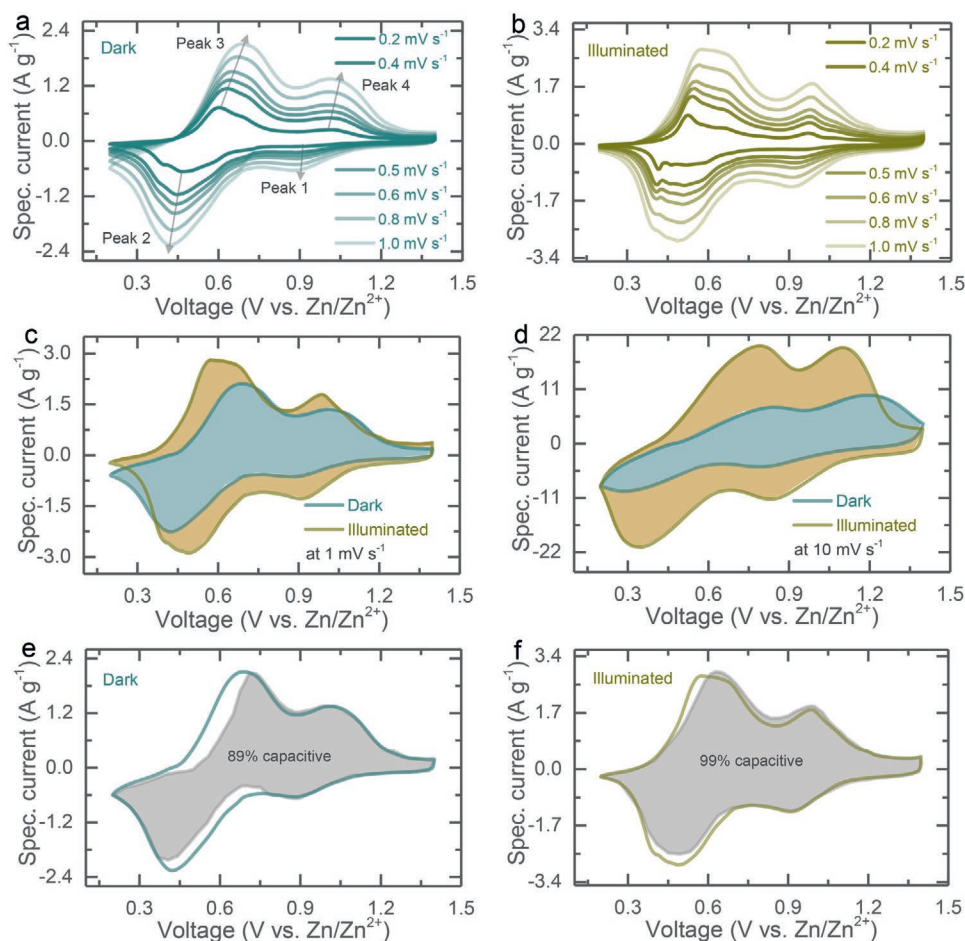
ADVANCED
SCIENCE NEWS
www.advancedsciencenews.com

ADVANCED
ENERGY
MATERIALS
www.advenergymat.de

Figure 3. CV curves of photo-ZIBs at different scan rates of 0.2–1.0 mV s^{-1} in a) dark and b) illuminated conditions. c,d) CV profiles at scans of 1.0 and 10 mV s^{-1} in both dark and illuminated conditions. e,f) Capacitive contribution calculations to charge storage at scan rate of 1.0 mV s^{-1} in dark and illuminated conditions.

of 2–8 mV s^{-1} in dark and illuminated conditions. To understand the light-induced photocathode capacity enhancement better, we quantify the capacity contributions from capacitive-controlled and diffusion-controlled mechanisms. In principle, the peak current (i) of CV curves follows a power-law relation with the scan rate (v) according to the equation,[19,20]

$$i = a v^b \tag{1}$$

or

$$\log(i) = \log(a) + b \times \log(v) \tag{2}$$

where, a and b are variable parameters. The b values for cathodic and anodic peaks can be calculated from the slopes of log (v) versus log (i) curves and are typically in the range of 0 to 1. A value of $b \approx 0.5$ indicates a diffusion-controlled electrochemical process, whereas a value of $b \approx 1.0$ indicates a capacitive-controlled dominant process.[19] As shown in Figure S7, Supporting Information, the calculated b-values for Peak 1, Peak 2, Peak 3, and Peak 4 are measured to be 0.93, 0.67, 0.58, and 0.94, respectively in the dark. This implies contributions from both diffusive and capacitive processes.[17] However, under illumination, the b-values increase

to 1.0, 0.89, 0.83, and 1.0, respectively, suggesting that under light exposure, the capacitive contributions are dominating.

Further, the charge storage process can be quantified into capacitive-controlled (k_1v) and diffusion-controlled ($k_2v^{1/2}$) components following the current at a fixed voltage relation,[21]

$$i(V) = k_1 v + k_2 v^{1/2} \tag{3}$$

or

$$i(V)/v^{1/2} = k_1 v^{1/2} + k_2 \tag{4}$$

Using this relation, calculate the overall capacitive contribution to be ≈89% in dark conditions (Figure 3e), and this increases to ≈99% under illumination (Figure 3f). Therefore, upon illumination, the photogenerated charges synergistically improve the capacitive contribution of the photocathodes, resulting in significantly faster zinc ion diffusion kinetics.

Further, the peak currents of the CV curves can be correlated with the zinc ion diffusion constant (D) as follows,

$$i_p = 0.4463F\left(F/RT\right)^{1/2} C^* v^{1/2} A D^{1/2}$$
$$= K v^{1/2} D^{1/2} \tag{5}$$

2100115 (4 of 8)

**ADVANCED
SCIENCE NEWS**
www.advancedsciencenews.com
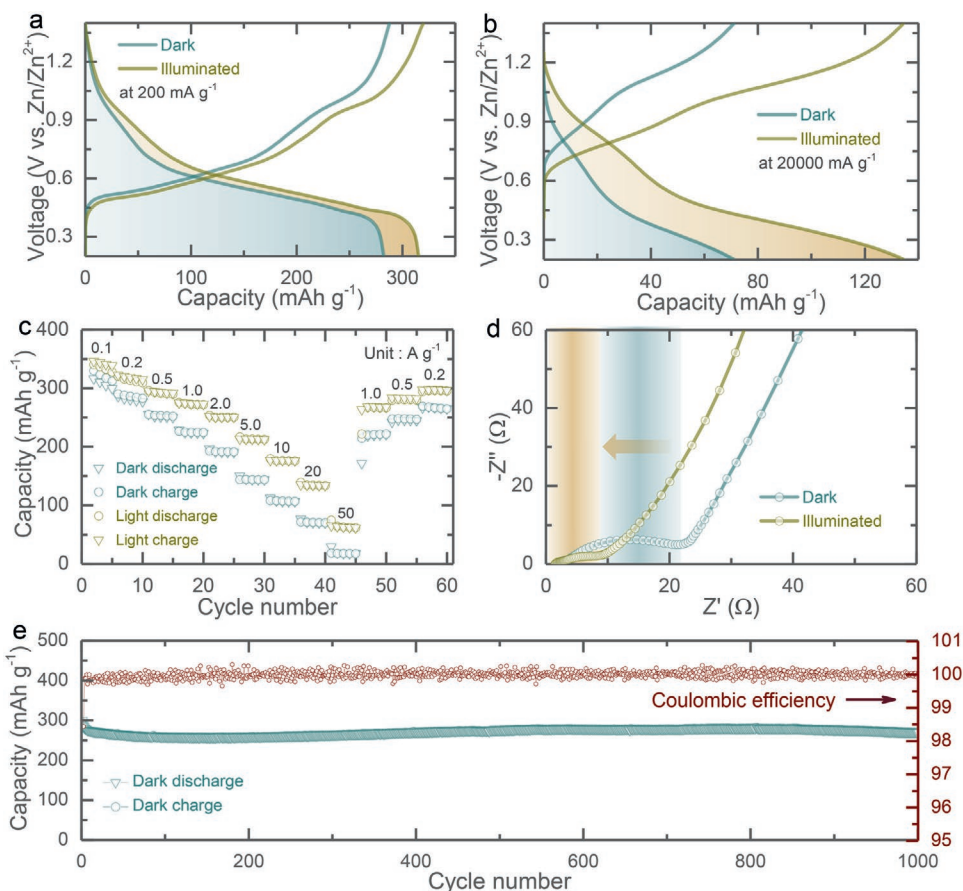
**ADVANCED
ENERGY
MATERIALS**
www.advenergymat.de

Figure 4. a,b) Galvanostatic discharge–charge curves at specific currents of 200 and 20,000 mA g^{-1} in dark and illuminated conditions after formation cycle. c) Rate capacity tests of the photo-ZIBs in dark and illuminated conditions. d) AC impedance spectra of the photo-ZIB acquired after the 2nd galvanostatic discharge cycle to 0.7 V in the frequency range of 10 mHz–100 kHz at 10 mV amplitude, comparing the impedance response under dark and illuminated conditions. e) Long-term cycling test of the photo-ZIB at a specific current of 1000 mA g^{-1} in dark.

where, i_p represents peak current, C^* the initial concentration (mol cm^{-3}), v the scan rate (V s^{-1}), F the Faraday constant, A the electrode area (cm^2) and $K = 0.4463F\ (F/RT)^{1/2}\ C^*$ is a constant.[22] By considering the slope of $v^{1/2}$ plotted against i_p/K in dark and then in illuminated conditions, the relative change in diffusion constants can be compared. Assuming the electrode area is not affected by illumination, the diffusion constants are increased by ≈40%/≈157% for the cathodic Peak 2 and by ≈41%/≈246% for the anodic Peak 3 (at scan rate ranges of 0.2–1.0 mV s^{-1}/2.0–10 mV s^{-1} see Figure S8, Supporting Information).

To evaluate the electrochemical performance of the photo-ZIBs, we measure the galvanostatic discharge–charge at different specific currents ranging from 100 to 50 000 mA g^{-1} under dark and illuminated conditions. As expected from the CV curves, the capacities of the photo-ZIBs are enhanced under illumination, for instance, the capacity increases from 282 to 315 mAh g^{-1} (11.7% enhancement) at 200 mA g^{-1} (**Figure 4**a) and from 71 to 134 mAh g^{-1} (88.7% enhancement) at higher specific currents of 20,000 mA g^{-1} (Figure 4b). This suggests that light can not only be used to recharge batteries but also to increase high-rate performance, which is in agreement with the increase in zinc-ion diffusion discussed above. The dQ/dV curves in light and dark conditions are provided in Figures S9 and S10,

Supporting Information, shows additional galvanostatic discharge–charge curves at 500, 1000, 5000, and 10,000 mA g^{-1} in both dark and illuminated conditions and these results are summarized in the rate test shown in Figure 4c. At extremely high current densities of 50,000 mA g^{-1} (i.e., a rate of ≈250 C based on the capacity in dark conditions), the photo-ZIBs retain a capacity of 65 mAh g^{-1} when illuminated, whereas only 19 mAh g^{-1} is achieved in normal, dark operating conditions. This capacity enhancement of ≈242% using light at ultra-high current densities is probably due to the increase in capacitive contribution and faster zinc ions diffusion discussed above. Also electrochemical impedance spectroscopy (EIS) response of the photo-ZIBs in light and dark conditions (10 mHz–100 kHz, voltage amplitude 10 mV, recorded after the 2nd galvanostatic discharge cycle to 0.7 V) suggest better rate performances can be achieved under illumination. As shown in the Nyquist plots in Figure 4d (Figure S11, Supporting Information, shows respective equivalent circuits), the charge transfer resistance decreases from ≈22 to ≈8.9 Ω under illumination, which is in agreement with earlier reports on photo-rechargeable batteries.[5,13] Finally, Figure 4e shows that the ZIBs retain ≈92% of their capacity after 500 cycles and ≈90% after 1000 cycles. The coulombic efficiency is 98.4% in the first cycle, which then
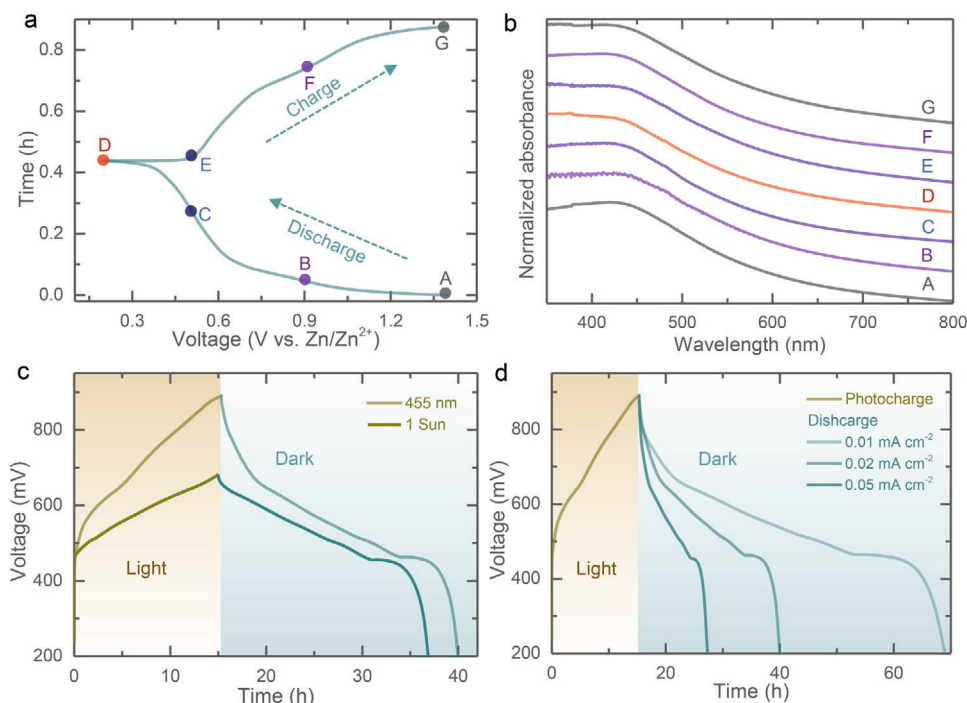
ADVANCED
SCIENCE NEWS
www.advancedsciencenews.com

ADVANCED
ENERGY
MATERIALS
www.advenergymat.de

Figure 5. a) Galvanostatic discharge–charge cycle of the optical-cell (2nd cycle). b) Ex situ absorbance spectra of the photo-ZIB cathode material at the states of charge denoted in (a). c) Photocharge cycles at $\lambda \approx 455$ nm and 1 sun (400–1100 nm, LED Solar Simulator LSH-7320) followed by discharging at same specific current of 0.02 mA cm^{-2} in dark to compare the effect of differing light-source exposure. d) Photocharge (light only, $\lambda \approx 455$ nm) of the photo-ZIB followed by discharges at different specific currents of 0.01, 0.02, and 0.05 mA cm^{-2} under dark conditions, probing the true amount of charge stored by the illumination.

achieves ≈99.9% after 15th cycle. Moreover, we tested the cycling stability of the photo-ZIB under light, showing capacity retention of ≈79% after 250 cycles at 5000 mA g^{-1} (see Figure S12a, Supporting Information). Figure S12b,c, Supporting Information shows SEM images of the photocathodes before and after cycling under illumination.

Ex situ UV–VIS measurements are used to investigate the bandgap evolution of the photocathodes during the discharging and charging processes. For these measurements, the photocathodes were dropcast onto FTO coated glass current collectors, instead of CF, and were then mounted into the optical-cells.[6] The material is then discharged and charged to the states of charge shown in **Figure 5**a. Figure 5b shows the UV–VIS absorbance spectra of the photocathodes these different state of charge, and given the shape of the curve is not changing substantially, it indicates that the insertion of zinc ions into VO$_2$ does not significantly alter the optical bandgap (transmittance spectra of the photocathodes are provided in Figure S13, Supporting Information). This observation differs from previous studies of V$_2$O$_5$ cathodes in LIBs, which incur significant changes to their optical bandgap during lithiation.[23] The resilience to change of the bandgap of VO$_2$ in this work, is deemed advantageous for the operation of ZIBs, where the absorbance profile of the material, and thus the photo-enhancement, is unchanged, regardless of the state of charge. This also explains why increases in current are observed under illumination throughout the voltage range used in the CV and galvanostatic curves reported above.

Finally, we galvanostatic discharge photo-ZIBs and then photocharge the batteries using light only (i.e., without applying an external current). As illustrated in Figure 5c, the voltage of the photo-ZIB increases to ≈890 mV when illuminated for 15 h, which can be increased to ≈1045 mV by prolonging illumination (Figure S14, Supporting Information). As mentioned earlier, the photogenerated electrons are transported from VO$_2$ to the CF current collector through the rGO due to the energetically favorable pathway and finally accumulate on the Zn anode. We assume that the photogenerated holes increase the oxidation state of vanadium, which results in the release of Zn^{2+} in the electrolyte ($Zn - VO_2 + 2h^+ \rightarrow Zn^{2+} + VO_2$). At the same time, the photogenerated electrons on Zn anode will reduce Zn^{2+} ($Zn^{2+} + 2e^- \rightarrow Zn$), and the combination of these processes results in photocharging. When using a solar simulator (1 sun), see Figure 5c, the light-charging effect is slower compared to the 455 nm light source for the equivalent radiative power, because a portion of the solar spectrum sits below the bandgap of VO$_2$ and therefore does not contribute to photocharge excitation. Figure 5d shows light charging experiments followed by conventional dark galvanostatic discharge cycles at different current densities. These measurements make it possible to quantify the charge stored during the light-charging process and calculate the photo-conversion efficiency (for 455 nm illumination) of the photo-ZIBs. This is calculated to be ≈0.18% using $\eta = E_{out}/E_{in} \times 100\%$, where, E_{out} represents the discharge energy output of the photo-ZIB and E_{in} denotes incident light energy (see calculation in the Supporting Information). This value is over an order of magnitude higher than the previously reported photo-rechargeable LIBs with efficiencies range from 0.03 to 0.06%,[6,15] but it is lower than that of our earlier reported on V$_2$O$_5$

photocathode based photo-ZIB,[5] however we believe that this can be further increased by altering the electrode morphology and composition. However, the VO_2 photo-ZIBs proposed in this work achieve a capacity that is about two times higher than the previously reported photo-ZIB, a more impressive rate capability and a greatly improved cycling stability ($\approx$90% capacity retention over 1000 cycles compared to $\approx$83% over 500 cycles) without the need for relatively expensive P3HT used in previous devices.[5]

In conclusion, this work demonstrates a light rechargeable ZIB with a high rate capability and long-term cycling stability (>1000 cycles), by using a simple combination VO_2 and rGO. Upon illumination, the generated charges not only allow for the photocharging of these cells, but also improve the capacity ($\approx$315 mAh g^{-1} at 200 mA g^{-1}) as well as the zinc ion diffusion kinetics. These photo-rechargeable systems are of interest for stand-alone energy harvesting and storage systems, which in turn are critical for powering off-grid communities and devices.

2. Experimental Section

Material Synthesis and Photocathode Preparation: First, 0.7 g of NH_4VO_3 was dispersed in 60 mL deionized (DI) water followed by magnetic stirring. Then, 4.8 mL formic acid was added into the above solution and continued stirring for another 1 h. The solution was transferred into Teflon-liners, which were placed on the microwave reactor followed by maintaining temperature at 200 °C for 520 min. Finally, the resulting VO_2 nanorods were washed with ethanol and DI water followed by drying at 60 °C.

For the preparation of the photocathodes, 91 mg of VO_2 nanorods and 4 mg of rGO were dispersed in 4 mL N-Methyl-2-pyrrolidone (Sigma-Aldrich) in an ultrasonic bath. Then, 5 mg PVDF (Solef 6020) binder was added. The photocathode solution was dropcasted on CF (Sigracet GDL 39 AA carbon graphite paper, SGL Carbon) current collectors and dried at 120 °C in vacuum oven for electrochemical measurements or FTO for optical analysis at various states of charge.

Material Characterization: The morphological and elemental analysis of VO_2 samples were characterized by SEM (FEI Magellan 400L) and TEM (Talos F200X G2). XRD (Bruker D8 Advance, Cu Kα radiation) was performed to analyze crystal structure. Moreover, the optical properties of the samples were characterized by using UV–VIS–NIR Spectrometer (Lamda 750).

Design of Photo-ZIBs: Coin cell (CR2450) type photo-ZIBs were designed by making an 8 mm hole in the coin cell casing, on the cathode side, and were then sealed with a glass window for illumination. Thinly cut carbon nanotube strips were used to connect the photocathode material electrically to the inside of the coin cell casing. Finally, a Whatman glass microfiber filters paper separator and 200 μL of 3 м $Zn(CF_3SO_3)_2$ (Sigma-Aldrich) aqueous electrolyte with metallic zinc (Zn, Alfa Aesar, 0.25 mm thick) anode were used to complete the full cell configuration based photo-ZIB device.

Electrochemical Tests: CV curves at different scan rates ranging from 0.1 to 10 mV s^{-1} over a working voltage range of 0.2 to 1.4 V were tested using a Biologic VMP-3 galvanostatic battery cycler in dark and illuminated conditions. For the illuminated conditions, an LED light source with wavelength, $\lambda \approx$455 nm and intensity $\approx$12 mW cm^{-2} was used. Likewise, galvanostatic discharge–charge measurements were extended at different specific currents range from 100 to 50,000 mA g^{-1} in dark and illuminated conditions. AC impedance (EIS) measurements of the photo-ZIB were taken in the frequency range of 10 mHz to 100 kHz at a 10 mV voltage amplitude in dark and illuminated states. Furthermore, the photocharging measurements were employed by recording open circuit voltage response (in the absence of an external current under light illumination) and the discharged by applying predetermined discharge currents.

Ex Situ UV–VIS Characterization: To measure the ex situ UV–VIS absorption and transmission of the photocathodes at different states of charge, the photocathodes were prepared by dropcasting on the FTO coated glass substrates (surface resistivity $\sim$7 Ω sq^{-1}, Sigma-Aldrich) and then cycled galvanostatically to different states of charge by applying a constant specific current.[6] The cycled optical-cells were then disassembled and washed with DI water followed by drying at 120 °C under vacuum. The optical absorption and transmission spectra of the photocathodes were acquired by using PerkinElmer UV/Vis/NIR Spectrometer (Lamda 750).

Fabrication of PDs and Electrical Measurements: The electrical photoresponse of VO_2 nanorods were tested by patterning gold (Au)/ Chromium (Cr) (40/10 nm) IDE on a Si_3N_4/Si wafer followed by UV lithography to pattern the contacts before and drop casting the VO_5 nanorods on the IDE. First, IV tests were measured by sweeping the potential from −1 to +1 V in dark and then illuminated conditions. Further, current–time measurements under alternative dark and illuminated states were recorded with an external bias of 1 V.

The stacked FTO/rGO/VO_2/Ag PD device was fabricated by dropcasting rGO and VO_2 sequentially on the FTO coated glass substrate followed by drying at $\approx$120 °C and then the deposition of Ag paste contacts. IV measurements (−1 to +1 V in dark and illuminated conditions) and current–time response measurements were taken under alternating dark and illuminated conditions in the absence of an external bias ($V = 0$ V).

Supporting Information

Supporting Information is available from the Wiley Online Library or from the author.

Conflict of Interest

The authors declare no conflict of interest.

Data Availability Statement

Research data are not shared.

[1] H.-D. Um, K.-H. Choi, I. Hwang, S.-H. Kim, K. Seo, S.-Y. Lee, *Energy Environ. Sci.* **2017**, *10*, 931.

[2] A. Gurung, K. M. Reza, S. Mabrouk, B. Bahrami, R. Pathak, B. S. Lamsal, S. I. Rahman, N. Ghimire, R. S. Bobba, K. Chen, J. Pokharel, A. Baniya, M. A. R. Laskar, M. Liang, W. Zhang,

**ADVANCED
SCIENCE NEWS**

www.advancedsciencenews.com

**ADVANCED
ENERGY
MATERIALS**

www.advenergymat.de

W.-H. Zhang, S. Yang, K. Xu, Q. Qiao, *Adv. Funct. Mater.* **2020**, *30*, 2001865.

[3] Z. Tian, X. Tong, G. Sheng, Y. Shao, L. Yu, V. Tung, J. Sun, R. B. Kaner, Z. Liu, *Nat. Commun.* **2019**, *10*, 4913.

[4] Z. Fang, X. Hu, D. Yu, *ChemPlusChem* **2020**, *85*, 600.

[5] B. D. Boruah, A. Mathieson, B. Wen, S. Feldmann, W. M. Dose, M. D. Volder, *Energy Environ. Sci.* **2020**, *13*, 2414.

[6] S. Ahmad, C. George, D. J. Beesley, J. J. Baumberg, M. D. Volder, *Nano Lett.* **2018**, *18*, 1856.

[7] A. Paolella, A. Vijh, A. Guerfi, K. Zaghib, C. Faure, *J. Electrochem. Soc.* **2020**, *167*, 120545.

[8] N. F. Yan, G. R. Li, X. P. Gao, *J. Mater. Chem. A* **2013**, *1*, 7012.

[9] Y. Liu, N. Li, S. Wu, K. Liao, K. Zhu, J. Yia, H. Zhou, *Energy Environ. Sci.* **2015**, *8*, 2664.

[10] Q. Lv, Z. Zhu, S. Zhao, L. Wang, Q. Zhao, F. Li, L. A. Archer, J. Chen, *J. Am. Chem. Soc.* **2021**, *143*, 1941.

[11] X. Xie, Z. Fang, M. Yang, F. Zhu, D. Yu, *Adv. Funct. Mater.* **2021**, 2007942, https://doi.org/10.1002/adfm.202007942.

[12] B. D. Boruah, A. Mathieson, B. Wen, C. Jo, F. Deschler, M. D. Volder, *Nano Lett.* **2020**, *20*, 5967.

[13] B. D. Boruah, B. Wen, S. Nagane, X. Zhang, S. D. Stranks, A. Boies, M. D. Volder, *ACS Energy Lett.* **2020**, *5*, 3132.

[14] O. Nguyen, E. Courtin, F. Sauvage, N. Krins, C. Sanchez, C. Laberty-Robert, *J. Mater. Chem. A* **2017**, *5*, 5927.

[15] A. Paolella, C. Faure, G. Bertoni, S. Marras, A. Guerfi, A. Darwiche, P. Hovington, B. Commarieu, Z. Wang, M. Prato, M. Colombo, S. Monaco, W. Zhu, Z. Feng, A. Vijh, C. George, G. P. Demopoulos, M. Armand, K. Zaghib, *Nat. Commun.* **2017**, *8*, 14643.

[16] L. Chen, Y. Ruan, G. Zhang, Q. Wei, Y. Jiang, T. Xiong, P. He, W. Yang, M. Yan, Q. An, L. Mai, *Chem. Mater.* **2019**, *31*, 699.

[17] Z. Li, S. Ganapathy, Y. Xu, Z. Zhou, M. Sarilar, M. Wagemaker, *Adv. Energy Mater.* **2019**, *9*, 1900237.

[18] J. Ding, Z. Du, L. Gu, B. Li, L. Wang, S. Wang, Y. Gong, S. Yang, *Adv. Mater.* **2018**, *30*, 1800762.

[19] V. Augustyn, J. Come, M. A. Lowe, J. W. Kim, P.-L. Taberna, S. H. Tolbert, H. D. Abruña, P. Simon, B. Dunn, *Nat. Mater.* **2013**, *12*, 518.

[20] B. K. Lesel, J. S. Ko, B. Dunn, S. H. Tolbert, *ACS Nano* **2016**, *10*, 7572.

[21] J. Wang, J. Polleux, J. Lim, B. Dunn, *J. Phys. Chem. C* **2007**, *111*, 14925.

[22] D. Y. W. Yu, C. Fietzek, W. Weydanz, K. Donoue, T. Inoue, H. Kurokawa, S. Fujitani, *J. Electrochem. Soc.* **2007**, *154*, A253.

[23] Q. Wang, M. Brier, S. Joshi, A. Puntambekar, V. Chakrapani, *Phys. Rev. B* **2016**, *94*, 245305.

2100115 (8 of 8)